Signal Processing 89 (2009) 1061–1069

Contents lists available at ScienceDirect

Signal Processing

journal homepage: www.elsevier.com/locate/sigpro

Adaptive polarimetry design for a target in compound-Gaussian clutter ☆

Jian Wang, Arye Nehorai *

Department of Electrical and Systems Engineering, Washington University in St. Louis, Bryan 201, Box 1127, 1 Brookings Drive, St. Louis, MO 63130, USA

ARTICLE INFO

Article history:
Received 10 April 2008
Received in revised form
6 November 2008
Accepted 16 December 2008
Available online 3 January 2009

Keywords:
Compound-Gaussian clutter
PX–EM algorithm
Cramer–Rao bound
Waveform design

ABSTRACT

We develop optimal adaptive design of radar waveform polarizations for a target in compound-Gaussian clutter. We present maximum likelihood estimates of the target's scattering matrix and clutter parameters using a parameter-expanded expectation-maximization (PX-EM) algorithm. We compute the Cramér–Rao bound (CRB) on the target's scattering matrix. To design the polarization, we propose an algorithm that minimizes a CRB function. We propose also suboptimal versions of this algorithm and illustrate the performance as well as compare our algorithm with numerical examples.

1. Introduction

The problem of optimally selecting the polarization state of radar transmitted waveforms is of interest as it can improve the radar performance in target detection, tracking and identification, as well as mitigate the multi-path interference. An optimal polarization state selection approach was first considered in [1], which enables treating symmetric, asymmetric, monostatic, and bistatic cases in an identical way, see also [2]. The optimization in [1,2] is in the sense of maximizing the voltage at the receiving antenna under the assumption that the scattering matrix S is known, see [2–4] and Section 2. However, in practice, the scattering matrix of the target of interest is usually unknown because the target is either completely unknown or its posture is unknown.

Additionally, the backscattered clutter from the unsteady environment, such as sea surface and foliage covered terrain, is typically non-Gaussian, see [5–9], which makes it more challenging to estimate the scattering matrix accurately. In [10], Farina et al. gave an extensive review about the clutter modeling for high resolution radar. In [11], the authors were first to identified the important role of the reciprocal of local clutter power in signal detection and estimation against compound-Gaussian clutter. In [12,13], the authors investigated the structure of the polarimetric covariance matrix and discussed the optimal polarimetry design to increase the performance of detection under non-Gaussian clutter.

Currently there is intense interest in waveform design, fueled in part by recent advances in sensor information processing and related hardware, such as digital waveform modulators that make it feasible to implement pulse-to-pulse waveform selection in real-time.

It is worth observing that, in the modern statistical sea-clutter literature, the small-scale structure scattering of the two-scale model is termed *speckle* [10–16]. Variations of the local power, due to the amplitude modulation of the speckle introduced by the tilting of the small-scale

☆ This work was supported by the Department of Defense under the Air Force Office of Scientific Research MURI Grant FA9550-05-1-0443, AFOSR Grant FA9550-05-1-0018, DARPA funding under NRL Grant N00173-06-1-G006 and ONR Grant N000140810849.

* Corresponding author. Tel.: +1 314 935 7565.
E-mail address: nehorai@ese.wustl.edu (A. Nehorai).

0165-1684/$ - see front matter © 2008 Elsevier B.V. All rights reserved.
doi:10.1016/j.sigpro.2008.12.018

structure, are modeled as a random slow-varying process referred to as *texture*. According to this model, referred to as compound Gaussian, the complex envelope of sea clutter can then be written as the product of fast and slow components

$$\boldsymbol{e}(t) = \sqrt{u(t)}\boldsymbol{\chi}(t). \tag{1}$$

The fast components $\boldsymbol{\chi}(t)$, the *speckle*, accounts for local backscattering. It is assumed to be a stationary complex Gaussian process with zero mean, whose covariance matrix Σ is unknown. The slow-changing component $u(t)$, *texture*, describes the underlying power level of the data, which is a non-negative real random process. Due to their different physical origins, these two components are modeled with very different correlation lengths.

For X-band high-resolution sea-clutter data, the speckle correlation length was measured to be on the order of milliseconds, while the texture was on the order of seconds. Because of its long correlation time, in many references on radar the texture is modeled as a degenerated process, i.e., it has been considered constant within each coherent processing interval (CPI), changing according to a given probability density function (pdf) from on CPI to the other. This assumption is reasonable for radar processing times that is not too large and gives rise, for instance, to the well-known Weibull and models [6,14] and [17]. According to this assumption, The texture $u(t)$ is modeled as a stationary non-negative real random process with unknown shape parameter v.

In this paper (see also [18]), we consider adaptive optimal waveform design for polarized signals under compound-Gaussian clutter models with inverse gamma distributed texture, which is often used to model clutter in high-resolution and low-grazing-angle radar, see [19,16,21]. Note that there are some pioneer work for K-distributed clutter model, e.g., [19,22,23], which is a special case of compound-Gaussian model. We assume $u(t)$ follows the inverse gamma texture distribution because of the simplicity in its computation, see [19,20], and [22,24,25]. It has been shown to fit well real data in [25].

We illustrate the proposed concept of adaptive polarimetry design in Fig. 1. The transmitted polarized signal is scattered by the target and environment. At the receiver end, measurements of the sum of the scattered signal from the target and the interference from the environment (clutter) are obtained. Using these measurements, we estimate the parameters of both the target and the environment, and optimally choose the signal variables for the transmission to achieve the best system performance. We develop optimal adaptive design of polarized signals fitting the estimated target to get the best estimation performance of the scattering matrix. First we compute the maximum likelihood (ML) estimate of the scattering matrix S using a parameter-expanded expectation-maximization (PX–EM) algorithm, see [26]. We compute also the Cramér–Rao bound (CRB) on S and use it as the performance measure for the optimal design. Then we design algorithms to optimally or suboptimally select the polarization state parameters for the next transmitted signals under the criterion of minimizing the CRB.

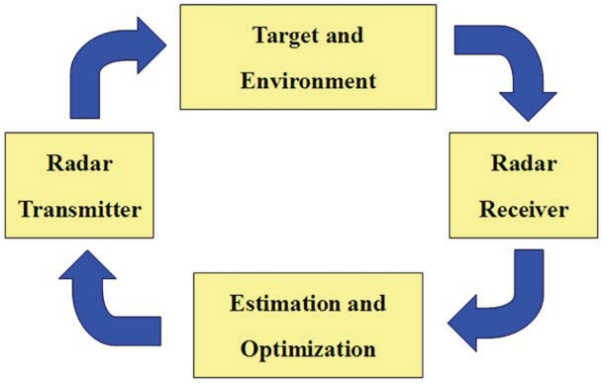

Fig. 1. Polarized radar waveform optimization block diagram.

This paper is organized as follows. In Section 2, we introduce the polarized radar signal measurement model. In Section 3, we present the ML estimates of the scattering matrix S, speckle covariance matrix Σ and texture distribution parameter v. In Section 4, we first compute the CRB on S, then present the algorithms for designing the polarization state of the transmitted waveform. We evaluate the performance of these algorithms with numerical examples in Section 5.

2. Measurement model

In this section, we present our parametric measurement model of a polarized signal with additive compound-Gaussian distributed clutter. To focus the discussion on the adaptive design process, we consider the simple coherent one-transceiver-antenna case (monostatic). We assume that the target is an ideal point scatterer in far field, which is stationary during the observation time and that the target's range, r, and direction are known.

Let $\boldsymbol{\xi}(t) = [\xi_h(t), \xi_v(t)]^T$ be the transmitted (incident) polarized electric field impinging on the target, and $\boldsymbol{y}(t) = [y_h(t), y_v(t)]^T$ be the complex envelope of the received (scattered) electric field, where the subscripts "h" and "v" denote the horizontal and vertical polarization components of a fully polarized signal, and the superscript "T" denotes the transpose. Under the far-field assumption, the scattered filed is related to the incident field by [2,27,28]

$$\boldsymbol{y}(t) = g(r)S\boldsymbol{\xi}(t) + \boldsymbol{e}(t), \quad t = 1, 2, \ldots, N, \tag{2}$$

where r denotes the range from the transmitting antenna to the target, S is the 2×2 scattering matrix, and $\boldsymbol{e}(t)$ denotes additive clutter. For simplicity, we ignore the measurement noise here. Assume $\boldsymbol{e}(t) = [e_h(t), e_v(t)]^T$ to be independently identical distributed (i.i.d.), under compound-Gaussian with parameters Σ and v. The variable N is the number of temporal observations. Denoting the wave number of the carrier waveform by k, we have $g(r) = e^{-2jkr}/2kr$ corresponding to the propagation magnitude attenuation and phase shift, which is a (known) complex scalar. We will estimate the

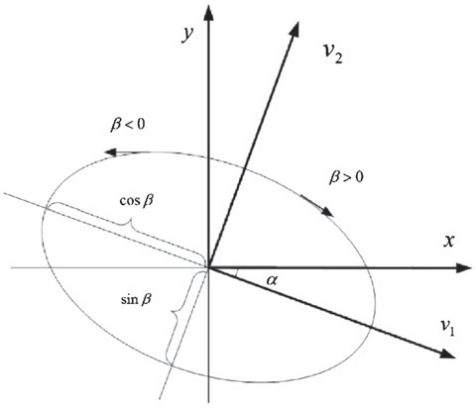

Fig. 2. Electric polarization ellipse.

scattering matrix of the target

$$S=\begin{bmatrix} s_{\mathrm{hh}} & s_{\mathrm{hv}} \\ s_{\mathrm{vh}} & s_{\mathrm{vv}} \end{bmatrix}, \tag{3}$$

which characterizes the polarization features of the target [4,27,28]. The first and second subscripts of each element in S denote the polarization components in the receiving and transmitting signals, respectively. For the reciprocal monostatic case, we can assume $s_{\mathrm{hv}}=s_{\mathrm{vh}}$.

We parameterize the transmitted signal using the notations of [29] and [30] (omitting time index for notational simplicity)

$$\xi=\|\xi\|e^{j\varphi}Q\boldsymbol{w}, \tag{4}$$

where

$$Q=\begin{bmatrix} \cos\alpha & \sin\alpha \\ -\sin\alpha & \cos\alpha \end{bmatrix}, \quad \boldsymbol{w}=\begin{bmatrix} \cos\beta \\ j\sin\beta \end{bmatrix}, \tag{5}$$

$\|\xi\|e^{j\varphi}$ is the complex envelope of the source signal, α denotes the rotation angle between the system coordinates and the electric ellipse axes, and β determines the ellipse's eccentricity, see Fig. 2. The definition space of these parameters are: $\|\xi\|$, $\varphi\in(-\pi,\pi]$, $\alpha\in(-\pi/2,\pi/2]$, $\beta\in[-\pi/4,\pi/4]$. Considering that the transmitted signal is power-limited, we exclude $\|\xi\|$ out of the design by setting $\|\xi\|=1$, i.e.,

$$\xi=e^{j\varphi}\begin{bmatrix} \cos\alpha\cos\beta+j\sin\alpha\sin\beta \\ -\sin\alpha\cos\beta+j\cos\alpha\sin\beta \end{bmatrix}. \tag{6}$$

3. Scattering matrix estimation

The traditional way of measuring the scattering matrix of a given target is to transmit intermittently vertically and horizontally polarized signals and recording both components of the received wave. From the measurement, the scattering matrix is calculated by its definition. Previous work on measuring the scattering matrix assumes no interference (clutter) in the measurement [31]. In our work, we assume the clutter exists and is compound-Gaussian distributed. In the following, we estimate the scattering matrix under compound-Gaussian noise assumption.

We now propose the ML estimate for the scattering matrix S and clutter parameters Σ, v in the measurement model (2). By definition, the reciprocal of $u(t)$ follows a gamma distribution with mean one and unknown shape parameter v, i.e. the pdf of $u(t)$ is

$$p_u(u(t);v)=\frac{1}{\Gamma(v)}v^v u(t)^{-v-1}e^{-v/u(t)}\sim \mathrm{iGamma}(v,1/v), \tag{7}$$

where $\Gamma(\cdot)$ is the gamma function. The conditional distribution of $\boldsymbol{y}(t)$ given $u(t)$ is

$$p_{y|u}(\boldsymbol{y}(t)|u(t);S,\Sigma)=\exp\{-[\boldsymbol{y}(t)-g(r)S\xi(t)]^H[u(t)\Sigma]^{-1}\times[\boldsymbol{y}(t)-g(r)S\xi(t)]\}/|\pi u(t)\Sigma|. \tag{8}$$

Integrating out the unobserved data $u(t)$, we obtain a *closed-form* expression for the marginal pdf of $\boldsymbol{y}(t)$

$$p_y(\boldsymbol{y}(t);S,\Sigma,v)=\frac{\Gamma(v+2)}{|\pi\Sigma|\cdot\Gamma(v)\cdot v^2}\{1+[\boldsymbol{y}(t)-g(r)S\xi(t)]^H\Sigma^{-1}\times[\boldsymbol{y}(t)-g(r)S\xi(t)]/v\}^{-v-2}. \tag{9}$$

Since it is impossible to find a closed-form solution for the ML estimates of S, Σ and v from the observed data likelihood (9), we use expectation-maximization (EM) algorithm to find the ML estimates from the *complete data log-likelihood*, which is easier to manipulate mathematically. Define the *unobserved data* $w(t)=u(t)^{-1}$. Our goal is to find the estimates that maximize the *complete data log-likelihood*

$$\begin{aligned} L_c &= \sum_{t=1}^{N}[\ln p_{y|w}(\boldsymbol{y}(t)|w(t);S,\Sigma)+\ln p_w(w(t);v)] \\ &= -\sum_{t=1}^{N}w(t)[\boldsymbol{y}(t)-g(r)S\xi(t)]^H\Sigma^{-1}[\boldsymbol{y}(t)-g(r)S\xi(t)] \\ &\quad +(v+1)\sum_{t=1}^{N}\ln w(t)-v\sum_{t=1}^{N}w(t)-N\ln|\pi\Sigma|+N\ln\frac{v^v}{\Gamma(v)}. \end{aligned} \tag{10}$$

In [32], we propose an ML estimation algorithm for the general multivariate analysis of variance (GMANOVA) model using the PX–EM algorithm in [33]. The model (2) is a special GMANOVA model with spatio-temporal matrix $A=g(r)\cdot I$, where I is the 2×2 identity matrix. Thus, we simplify the computation of S in the proposed PX–M step as is stated later in this paper.

The estimation algorithm is composed of two loops. In the inner loop, the ML estimates of S and Σ are computed for a fixed v value using PX–EM algorithm. In the outer loop, we estimate v with the estimation results in inner step using alternate projection until v converges.

Estimating S and Σ: In the PX–E step, we calculate the conditional expectations of the complete-data sufficient statistics assuming all unknown parameters $\{S,\Sigma,v\}$ are known from the complete data log-likelihood. In the PX–M step, we estimate S and Σ from these expectations. The derivation of these estimates from the sufficient statistics are explained in [32] in details. With a fixed $v^{(j)}, j=1,2,\ldots,$ the resulting PX–EM algorithm

consists of iterating between the following PX–E and PX–M steps:

PX-E step: Here we compute the conditional expectations $\mathscr{T}_k(\hat{v}^{(j)}) = \mathrm{E}\{T_k(w;\hat{v}^{(j)})|\boldsymbol{y}\}$ of the sufficient statistics $T_k(\hat{v}^{(j)})$, $k=1,2,3$ for $\{S,\Sigma,v\}$. The sufficient statistics are computed from (10).

$$\hat{w}^{(i)}(t;v^{(j)}) = (v^{(j)}+2)\{v^{(j)} + [\boldsymbol{y}(t) - g(r)S^{(i)}\boldsymbol{\xi}(t)]^H \times [\Sigma^{(i)}]^{-1}[\boldsymbol{y}(t) - g(r)S^{(i)}\boldsymbol{\xi}(t)]\}^{-1} \tag{11a}$$

for $t=1,2,\ldots,N$ and

$$\mathscr{T}_1^{(i)}(\hat{v}^{(j)}) = \frac{1}{N}\cdot\sum_{t=1}^{N}\boldsymbol{y}(t)\boldsymbol{\xi}(t)^H\cdot\hat{w}^{(i)}(t;v^{(j)}), \tag{11b}$$

$$\mathscr{T}_2^{(i)}(\hat{v}^{(j)}) = \frac{1}{N}\cdot\sum_{t=1}^{N}\boldsymbol{y}(t)\boldsymbol{y}(t)^H\cdot\hat{w}^{(i)}(t;\hat{v}^{(j)}), \tag{11c}$$

$$\mathscr{T}_3^{(i)}(\hat{v}^{(j)}) = \frac{1}{N}\cdot\sum_{t=1}^{N}\boldsymbol{\xi}(t)\boldsymbol{\xi}(t)^H\cdot\hat{w}^{(i)}(t;\hat{v}^{(j)}). \tag{11d}$$

PX-M step: Compute the ML estimates using the conditional expectations of the sufficient statistics from the E step

$$\hat{S}^{(i+1)}(\hat{v}^{(j)}) = \frac{1}{g(r)}\mathscr{T}_1^{(i)}(\hat{v}^{(j)})(\mathscr{T}_3^{(i)}(\hat{v}^{(j)}))^{-1}, \tag{12a}$$

$$\hat{\Sigma}^{(i+1)}(\hat{v}^{(j)}) = [\mathscr{T}_2^{(i)}(\hat{v}^{(j)}) - \mathscr{T}_1^{(i)}(\hat{v}^{(j)})(\mathscr{T}_3^{(i)}(\hat{v}^{(j)}))^{-1}(\mathscr{T}_1^{(i)}(\hat{v}^{(j)}))^H] \Big/ \left[\frac{1}{N}\sum_{t=1}^{N}\hat{w}^{(i)}(t;\hat{v}^{(j)})\right], \quad i=1,2,\ldots. \tag{12b}$$

The above iteration is performed until $\hat{S}^{(i)}(\hat{v}^{(j)})$ and $\hat{\Sigma}^{(i)}(\hat{v}^{(j)})$ converge. Denote by $\hat{S}^{(\infty)}(\hat{v}^{(j)})$ and $\hat{\Sigma}^{(\infty)}(\hat{v}^{(j)})$ the estimates of $\hat{S}$ and $\hat{\Sigma}$ obtained upon convergence.

Estimating v: We compute the ML estimate of v by maximizing the observed-data concentrated log-likelihood function with respect to $\hat{S}^{(\infty)}(\hat{v}^{(j)})$ and $\hat{\Sigma}^{(\infty)}(\hat{v}^{(j)})$

$$\hat{v}^{(j+1)} = \arg\max_{v}\sum_{t=1}^{N}\ln p_y(\boldsymbol{y}(t);\hat{S}^{(\infty)}(\hat{v}^{(j)}),\hat{\Sigma}^{(\infty)}(\hat{v}^{(j)}),v), \tag{13}$$

see also (9). Next we estimate S and Σ using this new estimate of $\hat{v}^{(j+1)}$, etc.

4. Optimal waveform parameter selection

Since the estimation algorithm we use is ML, its asymptotical accuracy is expected to attain the CRB. So by minimizing the CRB cost-function with respect to the transmitted signal, we will minimize the corresponding asymptotic estimation error. We will then choose the polarization state that minimizes the CRB to be transmitted in the next pulse. Thus, in this section we will consider the optimal polarization design subject to minimizing the CRB function.

4.1. Cramér–Rao bound

In [33], we proved that the clutter parameters and target parameters are decoupled, i.e., the mutual information between the clutter and target parameters are zero. Hence we use the result of the block for target parameter in CRB matrix directly, assuming the clutter parameters are known. Define the vector of parameters of interest

$$\boldsymbol{\rho} = [\mathrm{Re}\{\mathrm{vech}(S)\}^{\mathrm{T}}, \mathrm{Im}\{\mathrm{vech}(S)\}^{\mathrm{T}}]^{\mathrm{T}}, \tag{14}$$

where the "vech" matrix operator creates a single column vector by stacking elements below (including) the main diagonal columnwise. Considering that $s_{\mathrm{hv}} = s_{\mathrm{vh}}$, then $\boldsymbol{\rho}$ is a 6×1 vector and the CRB with respect to $\boldsymbol{\rho}$ is a 6×6 matrix. We minimize the determinant of the CRB matrix, which is also known as the D-optimality criterion [34]. This is equivalent to maximizing the determinant of the Fisher information matrix (FIM), whose elements are

$$[I(\boldsymbol{\rho};\Sigma)]_{pq} = \frac{2(v+2)}{v+3}\sum_{t=1}^{N}\left[\left(g(r)\frac{\partial S}{\partial\rho_p}\boldsymbol{\xi}(t)\right)^H\cdot\Sigma^{-1} \times g(r)\frac{\partial S}{\partial\rho_q}\boldsymbol{\xi}(t)\right] \tag{15a}$$

$$= \frac{2(v+2)\|g(r)\|^2}{v+3}\mathrm{Re}\left[\sum_{t=1}^{N}\boldsymbol{\xi}(t)^H\frac{\partial S^H}{\partial\rho_p}\cdot\Sigma^{-1} \times\frac{\partial S}{\partial\rho_q}\boldsymbol{\xi}(t)\right]. \tag{15b}$$

Hence, the FIM can be expressed as

$$I(\boldsymbol{\rho};\Sigma) = \frac{2(v+2)\|g(r)\|^2}{v+3}\sum_{t=1}^{N}F(\alpha_t,\beta_t,\Sigma,\boldsymbol{\rho}), \tag{16}$$

where $F(\alpha_t,\beta_t,\Sigma,\boldsymbol{\rho})$ is the contribution of the tth signal to the FIM. The (p,q)th entry of $F(\alpha_t,\beta_t,\Sigma,\boldsymbol{\rho})$ has the form

$$[F(\alpha_t,\beta_t,\Sigma,\boldsymbol{\rho})]_{pq} = \mathrm{Re}\left(\boldsymbol{\xi}(t)^H\cdot\frac{\partial S^H}{\partial\rho_p}\Sigma^{-1}\frac{\partial S}{\partial\rho_q}\cdot\boldsymbol{\xi}(t)\right). \tag{17}$$

We now discuss the properties of FIM with respect to the transmitted signal.

Property 1. *The initial signal phase φ does not affect the FIM.*

Proof. Substituting the right side of (6) into (15b), we find that the FIM is independent of the initial phase φ, namely φ_{opt} can be arbitrarily selected in $(-\pi,\pi]$ without affecting the estimation performance. □

Property 2. *For $N=1$, the determinant of FIM equals zero.*

Considering that the covariance matrix of the speckle is Hermitian, and so is its inverse, we denote the inverse of the current estimate of the speckle covariance matrix as

$$\Sigma^{-1} = \begin{bmatrix} a_1 & a_2 - \mathrm{j}b_2 \\ a_2 + \mathrm{j}b_2 & a_3 \end{bmatrix} \tag{18}$$

where $a_1,a_2,a_3,b_2\in\mathbb{R}$. Substitute (4) and (18) into (17). It is straightforward to find that the determinant of $F(\alpha_t,\beta_t,\Sigma,\boldsymbol{\rho})$ equals zero despite the polarization state

$\{\alpha_t, \beta_t, \varphi\}$ of the transmitted signal. Hence, the determinant of the FIM equals zero in this case. Note that the dimension of the scattering matrix S is 2×2 and the transmitted signal $\boldsymbol{\xi}(t)$ is a 2×1 vector. The returned single signal will not enable identifying the scattering matrix.

An interesting observation is that if the transmitted polarized waveforms are fixed in all N steps, the determinant of FIM will still be zero. That is, increasing the number of observations without changing the transmitted waveform will not improve the estimation quality—the non-identifiability will still exist [30].

4.2. Adaptive optimal polarization state design

We now present the proposed algorithm for optimal design of the radar waveform polarization state and then a suboptimal version, under the criterion of minimizing the CRB-based cost function. Note that the optimization process will automatically take into account the above problem of non-identifiability. Because the estimate of S changes in time (until it converges), the optimal signal selected based on S will also change every time.

Denote

$$J_N(\Sigma) = \sum_{t=1}^{N} F(\alpha_t, \beta_t, \Sigma, \boldsymbol{\rho}), \tag{19}$$

where $F(\alpha_t, \beta_t, \Sigma, \boldsymbol{\rho})$ denote the contribution of the transmitted signal $\boldsymbol{\xi}(\alpha_t, \beta_t)$ to the FIM.

4.2.1. Optimal polarization state design

This method includes the following three steps:

Step 1: Update Σ with the estimation from N observations (see Section 3), $\Sigma = \widehat{\Sigma}_N$.
Step 2: Calculate $J_N(\widehat{\Sigma}_N)$.
Step 3: Find the optimal value $\{\alpha^*_{N+1}, \beta^*_{N+1}\}$ within their definition space:

$$\{\alpha^*_{N+1}, \beta^*_{N+1}\} = \arg \max_{\{\alpha,\beta\} \in [-\pi/2, \pi/2) \times [-\pi/4, \pi/4]} \det[J_N(\widehat{\Sigma}_N) + F(\alpha, \beta, \widehat{\Sigma}_N, \boldsymbol{\rho})]. \tag{20}$$

4.2.2. Suboptimal polarization state design

Here, to reduce the computational complexity, we apply the updated value $\widehat{\Sigma}_N$ only when we compute the $F(\alpha_N, \beta_N, \Sigma)$, thus

Step 1: Update Σ with the estimation from N observations.
Step 2: Calculate $F(\alpha^*_N, \beta^*_N, \widehat{\Sigma}_N)$ with (4) and (17), where the optimal waveform parameters $\{\alpha^*_N, \beta^*_N\}$ of the Nth transmitted signal are used. Update $\widetilde{J}(\Sigma)$ with

$$\widetilde{J}_N(\widehat{\Sigma}_N) = \widetilde{J}_{N-1}(\widehat{\Sigma}_{N-1}) + F(\alpha^*_N, \beta^*_N, \widehat{\Sigma}_N), \tag{21}$$

where $\widetilde{J}_N(\Sigma)$ is an approximation of $J_N(\Sigma)$, and $\widehat{J}_1(\widehat{\Sigma}_1) = J_1(\widehat{\Sigma}_1)$.

Step 3: Find the optimal value $\{\alpha^*_{N+1}, \beta^*_{N+1}\}$ within their definition space

$$\{\alpha^*_{N+1}, \beta^*_{N+1}\} = \arg \max_{\{\alpha,\beta\} \in [-\pi/2, \pi/2) \times [-\pi/4, \pi/4]} \det[\widetilde{J}_N(\widehat{\Sigma}_N) + F(\alpha, \beta, \widehat{\Sigma}_N, \boldsymbol{\rho})]. \tag{22}$$

4.2.3. Block-signal polarization state design

We also consider the case of optimization with N_b consecutive temporal signal samples at a time. Here, the determinant of CRB after sending one whole block of N_b consecutive signals as the performance measurement. The design is based on the suboptimal procedure.

Step 1: Update Σ with the estimation from N observations.
Step 2: Update $\widetilde{J}_N(\Sigma)$ with the group of signals designed before:

$$\widetilde{J}_N(\widehat{\Sigma}_N) = \widetilde{J}_{N-N_b}(\widehat{\Sigma}_{N-N_b}) + \sum_{t=N-N_b+1}^{N} F(\alpha^*_t, \beta^*_t, \widehat{\Sigma}_N). \tag{23}$$

Step 3: Find the optimal value of $\{\alpha_{N+1}, \beta_{N+1}, \ldots, \alpha_{N+N_b}, \beta_{N+N_b}\}$.

$$\{\alpha_{N+1}, \beta_{N+1}, \ldots, \alpha_{N+N_b}, \beta_{N+N_b}\} = \arg \max \det\left[\widetilde{J}_N(\widehat{\Sigma}_N) + \sum_{t=N+1}^{N+N_b} F(\alpha_t, \beta_t, \widehat{\Sigma}_N)\right], \tag{24}$$

where the argument is with respect to $\{\alpha_{N+1}, \beta_{N+1}, \ldots, \alpha_{N+N_b}, \beta_{N+N_b}\}$.

The computational complexity of all three algorithms discussed in Section 4.2 are linear to the observation number N. However, they are highly depend on the maximum point search algorithm used in Step 3. If we use lattice search with l_α and l_β points in each dimension of the domain space of $\{\alpha, \beta\}$, the complexity will be $O(l_\alpha l_\beta N)$.

5. Numerical examples

We demonstrate the effectiveness of our algorithms through numerical examples. We set the true value of the scattering matrix to

$$S = \begin{bmatrix} 2\mathrm{j} & 0.5 \\ 0.5 & -\mathrm{j} \end{bmatrix}, \tag{25}$$

which is used also in [1] and [2]. The speckle covariance matrix Σ was generated using a model similar to that in [35, Section 2.6] with 1000 patches. The (p, q)th element of the covariance matrix of the speckle component was chosen as

$$\Sigma_{p,q} = \sigma^2 \cdot 0.9^{|p-q|} \exp[\mathrm{j}(\pi/2)(p-q)], \quad p, q = 1, 2. \tag{26}$$

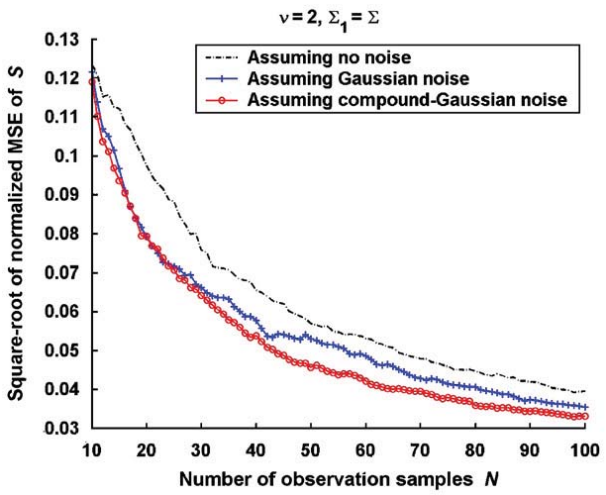

Fig. 3. Square-root of normalized mean-square errors of estimating the elements of the scattering matrix S for three different noise assumptions: (i) no noise, (ii) Gaussian noise, and (iii) compound-Gaussian noise, where $\nu = 2$, $\Sigma_1 = \Sigma$.

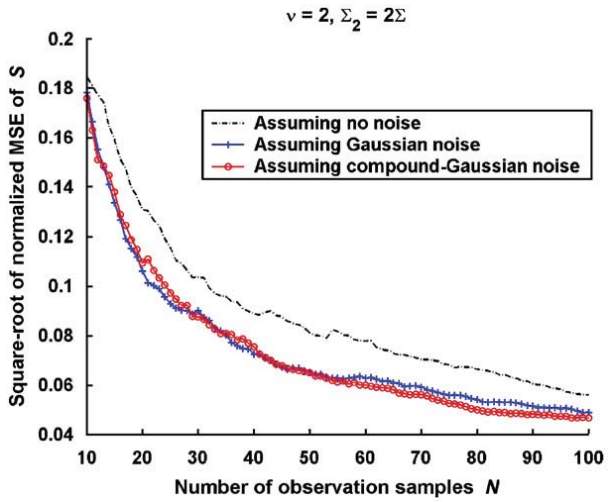

Fig. 4. Square-root of normalized mean-square errors of estimating the elements of the scattering matrix S for three different noise assumptions: (i) no noise, (ii) Gaussian noise, and (iii) compound-Gaussian noise, where $\nu = 2$, $\Sigma_2 = 2\Sigma$.

In the examples presented here, we selected $\sigma^2 = 2.05$. In the following numerical examples, without specification, we set the speckle covariance matrix to the above value and the texture distribution parameter $\nu = 2$. Since we assume the target's range r and direction are known, the value of factor $g(r)$ will not affect the results.

Note that the PX–EM algorithm can only converge after a certain number of measurements. Hence, in order to start our adaptive design algorithms, we send some pilot signals. Here, the number of pilot signals is set to 10 and the pilot signal parameters are randomly selected in each realization.

In Fig. 3, we show the square-root of normalized MSEs of the S, which is calculated by averaging the ratio of the square-root of MSE of each estimate to its true value, entirely under three noise related assumptions. The actual scenario is set to that the scattered field from the target is contaminated by compound-Gaussian distributed noise. We first use the conventional method, i.e., we send intermittently changing vertical and horizontal polarized signals and assume no clutter noise in the measurement (e.g., see [27] and references therein). Then we assume the measurement is contaminated by Gaussian noise and estimate S based on this assumption, see Appendix A for details about the ML estimation algorithm. Note that in this case, we use the optimal polarization design algorithm in Section 4.2 to determine the polarization parameters for the next transmitted signal. We also show the square-root of normalized MSE of the ML estimate for S under compound-Gaussian noise assumption with our optimal design algorithm. The results show that the optimal polarization design algorithm under compound-Gaussian noise assumption has a smaller MSE value than the other two at every evaluation point.

To evaluate the effect of the clutter power and its non-Gaussian distribution to these optimal design schemes, we vary the power of the speckle and texture parameter ν. Fig. 4 shows the results of square-root of normalized MSEs

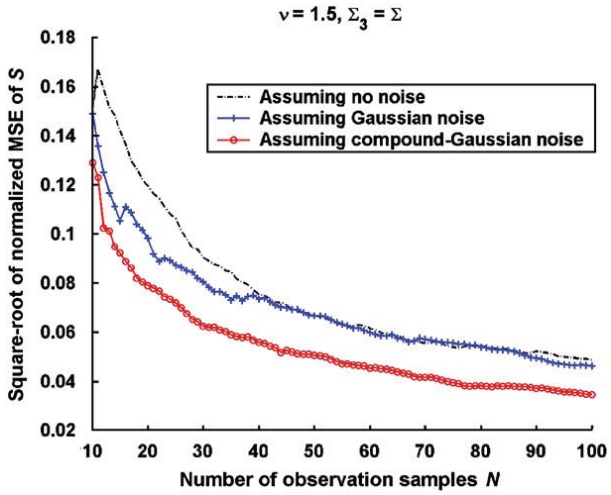

Fig. 5. Square-root of normalized mean-square errors of estimating the elements of the scattering matrix S for three different noise assumptions: (i) no noise, (ii) Gaussian noise, and (iii) compound-Gaussian noise, where $\nu = 1.5$, $\Sigma_3 = \Sigma$.

for the estimates of S with speckle covariance 2Σ. In Figs. 5 and 6, we show the results with $\nu = 1.5$ and 1, respectively. Observe that the value of ν indicate how much the clutter deviates from the Gaussian distribution. As $\nu \to \infty$, the inverse gamma texture distribution degenerates to a constant and, thus, the compound-Gaussian distributed clutter reduces to having complex Gaussian distribution [33]. We find that the power of clutter does not significantly affect the estimation results whereas a change in ν will significantly affect the estimation. In Fig. 5, the superiority of algorithm under the compound-Gaussian clutter assumption to algorithms under the other two noise assumptions increases. Interestingly, when the clutter deviates much from Gaussian

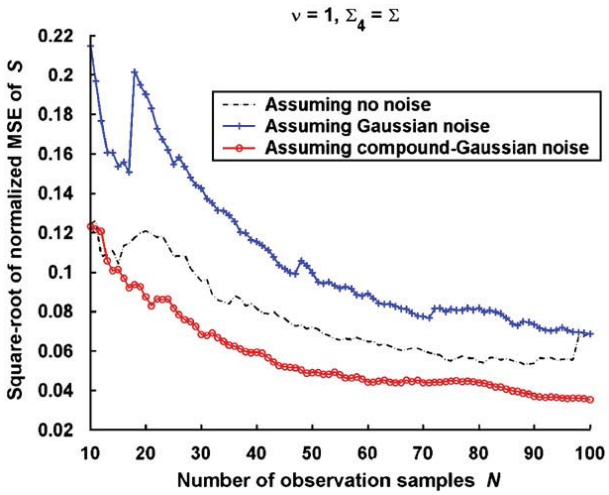

Fig. 6. Square-root of normalized mean-square errors of estimating the elements of the scattering matrix S for three different noise assumptions: (i) no noise, (ii) Gaussian noise, and (iii) compound-Gaussian noise, where $\nu = 1$, $\Sigma_4 = \Sigma$.

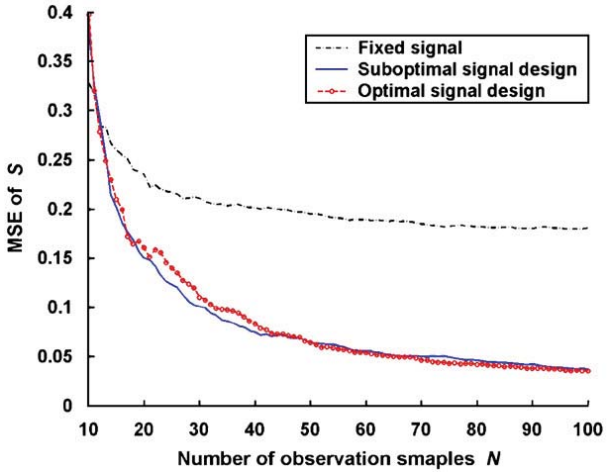

Fig. 7. Averaged mean-square errors of estimating the elements of the scattering matrix S for three different transmit signal schemes: (i) fixed signal, (ii) sub-optimal design, and (iii) optimal design.

distribution, i.e. $\nu = 1$, the Gaussian noise assumption leads to a worse performance even than the no noise assumption (see Fig. 6). From these results, it is obvious that the knowledge of the clutter distribution is much more important than that of the clutter energy in parameter estimation.

In Fig. 7, we show the average MSEs for the ML estimates of the scattering matrix entries over 50 independent trials as functions of N. Three different signal transmitting schemes are compared here: (i) fixed signal with $\alpha = \pi/3, \beta = \pi/6$, (ii) sub-optimally designed signal (see Section 4.2.2), and (iii) optimally designed signal (see Section 4.2.1). We vary the observation number from 10 to 100 in each scheme.

The results are shown in Fig. 7. Since at each step, the most efficient waveform (in terms of minimizing CRB) is

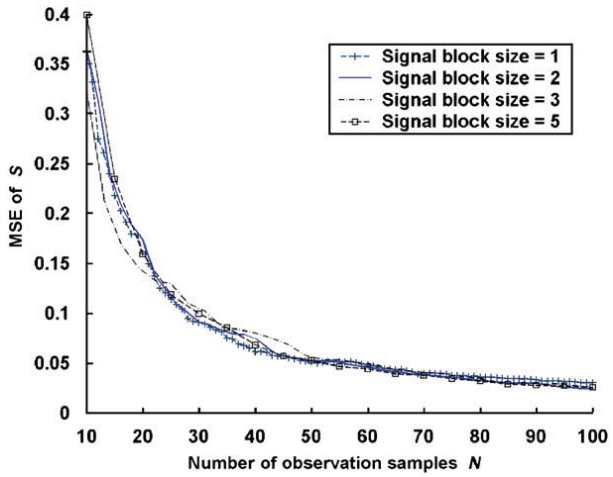

Fig. 8. Average mean-square errors of estimating the elements of scattering matrix S from suboptimal design algorithms of different block sizes vs. number of observations N.

selected, the result of optimal adaptive algorithm converges much faster than the other two when the number of observations increases. Both the optimally designed signal and the suboptimal one show significant improvement, the average MSE of $\widehat{S}$ decreases about 6 dB, comparing with the fixed signal. Note that the average MSE of $\widehat{S}$ is computed by averaging the MSE of each entries of S. The proposed suboptimal design algorithm has comparable performance to the optimal one.

In Fig. 8, we compare the MSEs of $\widehat{S}$ from optimizations with different block sizes, see Section 4.2.3. Here we choose the number of signals in a block to be $N_b = 1, 2, 3, 5$, respectively. The results show that when the observation lengths are large enough (larger than 50), i.e., we have enough information from the measurement to estimate S, the algorithm with bigger block size has a slightly better performance than ones with smaller block sizes.

6. Summary

We developed optimal adaptive design methods of radar waveform polarization state under compound-Gaussian clutter. We first presented the maximum-likelihood estimates for the scattering matrix and the clutter distribution parameters based on the parameter-expanded expectation-maximization algorithm. Then we computed the Cramér–Rao bound for the scattering matrix S and used it as the performance measure. By minimizing the CRB cost function, we optimally selected the polarization state parameters for the waveform to be transmitted in the next pulse. To decrease the computational load, we presented also a suboptimal version. An algorithm to optimize waveform variables for a block of signal was also developed. In the numerical examples, we compared the performance of these algorithms. The proposed algorithm shows a significant performance improvement in the estimation accuracy compared with the conventional methods. The proposed suboptimal

design algorithm has comparable performance to the optimal one. In the block-signal optimization, applying the algorithm using bigger block sizes slightly improves the performance. In the adaptive design procedure, the parameters estimation and the optimal parameter searching parts requires high computation power, which may preclude its real-time application.

Appendix A. Estimation of S under the Gaussian noise assumption

Model (2) under the Gaussian noise assumption is well investigated. Define $\boldsymbol{y}=[\boldsymbol{y}(1)^{\mathrm{T}},\boldsymbol{y}(2)^{\mathrm{T}},\ldots,\boldsymbol{y}(N)^{\mathrm{T}}]^{\mathrm{T}}$ and $\boldsymbol{e}=[\boldsymbol{e}(1)^{\mathrm{T}},\boldsymbol{e}(2)^{\mathrm{T}},\ldots,\boldsymbol{e}(N)^{\mathrm{T}}]^{\mathrm{T}}$. Denote the first and second entry of vector $\boldsymbol{\xi}(t)$ as $\xi_1(t)$ and $\xi_2(t)$, we can reform (2) into

$$\boldsymbol{y}=g(r)H\boldsymbol{s}+\boldsymbol{e}, \tag{A.27}$$

where

$$H=\begin{bmatrix}\xi_1(1) & \xi_2(1) & 0\\ 0 & \xi_1(1) & \xi_2(1)\\ & \vdots & \\ \xi_1(N) & \xi_2(N) & 0\\ 0 & \xi_1(N) & \xi_2(N)\end{bmatrix},\quad \boldsymbol{s}=\begin{bmatrix}s_{\mathrm{hh}}\\ s_{\mathrm{vh}}\\ s_{\mathrm{vv}}\end{bmatrix}. \tag{A.28}$$

Note that the scattering matrix S is symmetric by our assumption.

Thus the least squares estimator (LSE) of $\boldsymbol{s}$ is (see, e.g. [36, Chapter 8.4])

$$\hat{\boldsymbol{s}}=\frac{1}{g(r)}(H^{\mathrm{T}}H)^{-1}H^{\mathrm{T}}\boldsymbol{y}. \tag{A.29}$$

From the definition of $\boldsymbol{s}$, we can obtain the LSE of S

$$\widehat{S}=\begin{bmatrix}\hat{\boldsymbol{s}}(1) & \hat{\boldsymbol{s}}(2)\\ \hat{\boldsymbol{s}}(2) & \hat{\boldsymbol{s}}(3)\end{bmatrix}. \tag{A.30}$$

The ML estimator of the noise covariance matrix is

$$\widehat{\Sigma}=\frac{1}{N}[\boldsymbol{y}(t)-g(r)\widehat{S}\xi(t)][\boldsymbol{y}(t)-g(r)\widehat{S}\xi(t)]^{\mathrm{T}}. \tag{A.31}$$

Since the CRB of S under the Gaussian noise assumption is identical to the one under compound-Gaussian noise assumption (see [33] for details), the optimal and suboptimal polarization design algorithms in Section 4.2 are still effective for the Gaussian noise case.

References

[1] A.B. Kostinski, W.-M. Boerner, On foundations of radar polarimetry, IEEE Antennas Propag. AP-34 (December 1986) 1395–1404.

[2] W.-M. Boerner, W. Yan, A. Xi, Y. Ymaguchi, On the basic principles of radar polarimetry: the target characteristic polarization state theory of Kennaugh, Huynen's polarization form concept, and its extension to the partially polarized case, Proc. IEEE 79 (10) (October 1991) 1538–1550.

[3] E. M. Kennaugh, Effects of type of polarization on echo characteristics, Technical Reports 389-1 to 389-14, generated under sponsorship of Rome Air Development Center, the Ohio State University, Department of Electrical Engineering, Antenna Lab., September 1949–June 1952.

[4] N.E. Chamberlain, E.K. Walton, E.D. Garber, Radar target identification of aircraft using polarization-diverse features, IEEE Trans. Aerosp. Electron. Syst. 27 (1) (January 1991) 58–66.

[5] K.J. Sangston, K.R. Gerlach, Coherent detection of radar targets in a non-Gaussian background, IEEE Trans. Aerosp. Electron. Syst. 30 (April 1994) 330–340.

[6] D.C. Schleher, Radar detection in Weibull clutter, IEEE Trans. Aerosp. Electron. Syst. 12 (6) (1976) 736–743.

[7] D.R. Sheen, N.P. Malinas, D.W. Kletzli, T.B. Lewis, J.F. Roman, Foliage transmission measurements using a ground-based ultrawideband (UWB) (300–1300 MHz) SAR system, IEEE Trans. Geosci. Remote Sensing 32 (1) (1994).

[8] J.G. Fleischman, S. Ayasli, E.M. Adams, D.R. Gosselin, Foliage attenuation and backscatter analysis of SAR imagery, IEEE Trans Aerosp. Electron. Syst. 32 (1) (January 1996) 134–144.

[9] J.G. Fleischman, M.A. Worris, S. Ayasli, E.M. Adams, D.R. Gosselin, Multichannel whitening of SAR imagery, IEEE Trans Aerosp. Electron. Syst. 32 (1) (January 1996) 156–164.

[10] A. Farina, F. Gini, M. Greco, L. Verrazzani, High resolution sea clutter data: a statistical analysis of recorded live data, Proc. Inst. Electr. Eng. Part F 144 (3) (1997) 121C130.

[11] K.J. Sangston, F. Gini, M.V. Greco, A. Farina, Structures for radar detection in compound Gaussian clutter, IEEE Trans Aerosp. Electron. Syst. 35 (2) (April 1999) 445–458.

[12] P. Lombardo, D. Pastina, T. Bucciarelli, Adaptive polarimetric target detection with coherent radar part II: detection against non-Gaussian background, IEEE Trans Aerosp. Electron. Syst, 37 (4) (October 2001) 1207–1220.

[13] G. Alfano, A. De Maio, Adaptive polarimetric detection in compound-Gaussian clutter, in: Proceedings of the IEEE Radar Conference, May 5–8, 2003, pp. 102–109.

[14] T.J. Barnard, D.D. Weiner, Non-Gaussian clutter modeling with generalized spherically invariant random vectors, IEEE Trans. Signal Process. 44 (October 1996) 2384–2390.

[15] E. Conte, M. Longo, Characterization of radar clutter as a spherically invariant random process, Proc. Inst. Electr. Eng. Part F 134 (2) (1987) 191–197.

[16] T. Nohara, S. Haykin, Canadian east coast radar trials and the k-distribution, Proc. Inst. Electr. Eng. Part F F138 (2) (1991) 80–88.

[17] S. Haykin, R. Bakker, B.W. Currie, Uncovering nonlinear dynamics—the case study of sea clutter, Proc. IEEE 90 (May 2002) 860–881.

[18] J. Wang, A. Nehorai, Adaptive polarimetry design for a target in compound-Gaussian clutter, in: Proceedings of the International Waveform Diversity and Design Conference (WDD 06), Lihue, Hawaii, January 2006, 5pp.

[19] A. Dogandžić, A. Nehorai, J. Wang, Maximum likelihood estimation of compound-Gaussian clutter and target parameters, in: Proceedings of the 12th Annual Workshop Adaptive Sensor Array Processing (ASAP '04), Lincoln Laboratory, Lexington, MA, March 2004.

[20] J. Wang, A. Dogandžić, A. Nehorai, Cramer–Rao bounds for compound-Gaussian clutter and target parameters, in: IEEE International Conference on Acoustics, Speech, Signal Processing, Philadelphia, PA, March 2005, pp. 1101–1104.

[21] F. Gini, M.V. Greco, M. Diani, L. Verrazzani, Performance analysis of two adaptive radar detectors against non-Gaussian real sea clutter data, IEEE Trans. Aerosp. Electron. Syst. 36 (October 2000) 1429–1439.

[22] S. Watts, Radar detection prediction in K-distributed sea clutter and thermal noise, IEEE Trans Aerosp. Electron. Syst. 23 (1) (January 1987) 40–45.

[23] S. Watts, C.J. Baker, K.D. Ward, Maritime surveillance radar, part 2: Detection performance prediction in sea clutter, IEE Proc. Part F 137 (2) (April 1990) 63–73.

[24] K.L. Lange, R.J.A. Little, J.M.G. Taylor, Robust statistical modeling using the t distribution, J. Amer. Stat. Assoc. 84 (December 1989) 881–896.

[25] A. Balleri, A. Nehorai, J. Wang, Maximum likelihood estimation of compound-Gaussian clutter with inverse gamma texture, IEEE Trans. Aerosp. Electron. Syst. 43 (April 2007) 775–779.

[26] C.H. Liu, D.B. Rubin, Y.N. Wu, Parameter expansion to accelerate EM: the PX–EM algorithm, Biometrika 85 (December 1998) 755–770.

[27] W.M. Steedly, R.L. Moses, High resolution exponential modeling of fully polarized radar returns, IEEE Trans. Aerosp. Electron. Syst. 27 (3) (May 1991) 459–469.

[28] L.C. Potter, R.L. Moses, Attributed scattering centers for SAR ATR, IEEE Trans. Image Process. 6 (1) (January 1997) 79–91.

[29] A. Nehorai, E. Paldi, Vector–sensor array processing for electromagnetic source localization, IEEE Trans. Signal Process. SP-42 (April 1994) 376–398.

[30] B. Hochwald, A. Nehorai, Polarimetric modeling and parameter estimation with applications to remote sensing, IEEE Trans. Signal Process. SP-43 (August 1995) 1923–1935.
[31] F.T. Ulaby, K. Sarabandi, K. McDonald, M. Whitt, C. Dobson, Michigan microwave canopy scattering model, Int. J. Remote Sensing 11 (1990) 1223–1263.
[32] A. Dogandžić, A. Nehorai, Generalized multivariate analysis of variance: a unified framework for signal processing in correlated noise, IEEE Signal Process. Mag. 20 (September 2003) 39–54.
[33] J. Wang, A. Dogandžić, A. Nehorai, Maximum likelihood estimation of compound-Gaussian clutter and target parameters, IEEE Trans. Signal Process. 54 (October 2006) 3884–3898.
[34] G.E.P. Box, H.L. Lucas, Design of experiments in nonlinear situations, Biometrika 46 (1959) 77–90.
[35] J. Ward, Space-Time Adaptive Processing for Airborne Radar, Technical Report 1015, Lincoln Laboratory, MIT, December 1994.
[36] S.M. Kay, Fundamentals of Statistical Signal Processing: Estimation Theory, PTR Prentice-Hall, Inc., NJ, 1993.